**ELSEVIER**

**doi:10.1016/j.ultrasmedbio.2007.04.017**

● *Original Contribution*

# SIGNAL LOSSES WITH REAL-TIME THREE-DIMENSIONAL POWER DOPPLER IMAGING

DAMIEN GARCIA,* MARIANNE FENECH,[†] ZHAO QIN,[†] GILLES SOULEZ,[‡§] and
GUY CLOUTIER[†§]

*Laboratory of Biomedical Engineering, Clinical Research Institute of Montreal, University of Montreal;
[†]Laboratory of Biorheology and Medical Ultrasonics, Research Center, University of Montreal Hospital;
[‡]Department of Radiology, University of Montreal Hospital; and [§]Department of Radiology, Radio-Oncology and
Nuclear Medicine, and Institute of Biomedical Engineering, University of Montreal, Montreal, Quebec, Canada

**Abstract**—Power Doppler imaging (PDI) has been shown to be influenced by the wall filter when assessing arterial stenoses. Real-time 3-D Doppler imaging may likely become a widespread practice in the near future, but how the wall filter could affect PDI during the cardiac cycle has not been investigated. The objective of the study was to demonstrate that the wall filter may produce unexpected major signal losses in real-time 3-D PDI. To test our hypothesis, we first validated binary images obtained from analytical simulations with *in vitro* PDI acquisitions performed in a tube under pulsatile flow conditions. We then simulated PDI images in the presence of a severe stenosis, considering physiological conditions by finite element modeling. Power Doppler imaging simulations revealed important signal losses within the lumen area at different instants of the flow cycle, and there was a very good concordance between measured and predicted PDI binary images in the tube. Our results show that the wall filter may induce severe PDI signal losses that could negatively influence the assessment of vascular stenosis. Clinicians should therefore be aware of this cause of signal loss to properly interpret power Doppler angiographic images. (E-mail: guy.cloutier@umontreal.ca)    © 2007 World Federation for Ultrasound in Medicine & Biology.

*Key Words:* Power Doppler ultrasound imaging, Wall filter, Modeling, Arterial stenosis, Computational fluid dynamics, Finite element modeling.

## INTRODUCTION

Power Doppler imaging (PDI) was proposed in the 1990s and developed as an alternative to conventional color Doppler flow imaging (CDFI) for the evaluation of vascular pathologies (Rubin and Adler 1993; Rubin et al. 1994; Winsberg 1995). Power Doppler imaging produces color images based on a nonlinear map of the power of the Doppler signal and depends essentially on the erythrocyte scattering property within the sample volume (Rubin et al. 1994; Allard and Cloutier 1999) if no ultrasound (US) contrast agent is used. On the other hand, CFDI displays the flow velocity from the phase differences between transmitted and received echoes. Accordingly, PDI is less dependent on the angle of insonation,

is much less sensitive to noise and does not produce significant aliasing artifacts (Jain et al. 1991; Rubin et al. 1994; Allard et al. 1996; Rubin 1999). For these reasons, the flow information obtained from PDI has been analyzed widely *in vitro* and *in vivo* for the assessment of vascular stenoses in kidneys (Helenon et al. 1998; Manganaro et al. 2004; Kuwa et al. 2004), carotid arteries (Griewing et al. 1996; Steinke et al. 1996, 1997; Schmidt et al. 1998; Bluth et al. 2000; Koga et al. 2001; Muller et al. 2001; Poepping et al. 2002; Yurdakul et al. 2004), the coronary vasculature (Masugata et al. 2000, 2003; Villanueva et al. 2001; Rocchi et al. 2003) and lower limb arteries (Guo and Fenster 1996; Guo et al. 1998; Cloutier et al. 2000). Some investigators have shown that PDI better assesses the severity of arterial stenoses than CDFI (Steinke et al. 1996, 1997; Griewing et al. 1996; Villanueva et al. 2001; Manganaro et al. 2004) and may even give similar diagnostic as the X-ray angiographic method in high-grade stenoses (Steinke et al. 1997). Thus PDI is

nowadays considered as a powerful noninvasive tool, at least as a screening test (Bluth et al. 2000; Bluth 2001), for the diagnosis of arterial stenoses.

It has been reported, however, that PDI may also be greatly influenced by instrument settings, including the wall filter (Jain et al. 1991; Yoon et al. 1999; Mizushige et al. 1999; Cloutier et al. 2000; Claudon et al. 2001). The so-called wall filter is a high-pass filter applied to the Doppler signal to attenuate artifacts that may arise from the vessel wall motion. Wall filter settings are usually preset by the manufacturer and a high, medium or low wall filter is applied to PDI (Kruskal et al. 2004). During a typical clinical examination, a wall filter in the range of 50 to 800 Hz is chosen. In slow flow, the wall filter is kept at the lowest possible setting (in the 50–100 Hz range) to avoid excessive loss of signal. It was shown *in vitro* that the wall filter significantly affects the determination of the flow cross-sectional area when assessing the severity of an arterial stenosis, which may lead to the underestimation of the degree of stenosis (Jain et al. 1991; Cloutier et al. 2000; Claudon et al. 2001). These studies were performed either under continuous flow (Jain et al. 1991; Cloutier et al. 2000) or pulsatile conditions (Claudon et al. 2001). How the wall filter could affect PDI during the whole cardiac cycle has not yet been investigated. Because the temporal and spatial resolutions of Doppler instruments are incessantly improving, and because more robust signal processing algorithms are proposed for real-time imaging (Yu 2007), one may expect that instantaneous (*i.e.*, with no persistence) 3-D echography will become a widespread practice in the near future, especially for cardiac imaging (Claudon et al. 2002; Jones et al. 2003). More specifically, a few investigators recently studied some clinical potentials of electrocardiogram-gated or real-time PDI (Masugata et al. 2000, 2003; Nagao et al. 2002; Jones et al. 2003). The objective of this study was therefore to demonstrate that the wall filter can produce unexpected major signal losses on real-time 3-D PDI. To test our hypothesis, we first validated binary images obtained from analytical simulations with *in-vitro* flow-gated PDI acquisitions performed in a straight cylindrical tube under pulsatile flow conditions. We then simulated flow-gated PDI images for the case of a severe vessel stenosis by means of finite element modeling (FEM) and we quantitatively analyzed the effect of the wall filter on PDI.

## MATERIALS AND METHODS

### In-vitro *model*

The experiments were performed in a mock flow model at room temperature. The *in-vitro* model was previously described in detail (Cloutier et al. 2000), the only difference from our earlier study being the insertion of a parallel centrifugal pump (see below). It was composed of a wall-less cylindrical straight vessel whose inner diameter was 7.96 mm. A liquid made of 33% glycerol and of 66% saline water was used as a blood substitute. Its viscosity and density at room temperature were similar to that of blood under high shear rates (3.3 cP and 1080 kg/m$^3$, respectively). Cornstarches were added to the solution to provide US scatterers. The blood substitute was circulated at 60 beats/min with a pulsatile pump (Harvard Apparatus, model 1421, Holliston, MA, USA) coupled in parallel with a magnetic centrifugal pump (Micropump Inc., model 75225–10, Vancouver, WA, USA). The check valves of the Harvard pump were removed to produce periodic sinusoidal flows. The amplitude of the flow was regulated by changing the course of the pulsatile piston pump, whereas the mean flow rate was adjusted with the centrifugal pump. The resulting flow rate was measured with an electromagnetic flowmeter (Cliniflow II, Carolina Medical Electronics Inc, King, NC, USA). The flow waveform and the mean flow rate were not physiological in the *in-vitro* experiments. Indeed, we deliberately chose nonphysiologic sine-shaped flows to obtain a wide range of PDI image patterns, as illustrated in the results section.

### PDI *acquisition*

An ATL Ultramark 9 HDI US system (Philips Medical System, Bothell, WA, USA) with a 38-mm aperture linear-array probe (L7–4) was used for all PDI measurements. This probe was operated at 4 MHz in Doppler mode. The wall filter cutoff frequency was set at 50 or 100 Hz (low filter setting) and the Doppler angle was 70°. No persistence and no image filtering were selected. The pulse repetition frequency was adjusted in such a way that there was no aliasing in color flow (the aliasing is easier to see in color velocity mode than in power Doppler mode). The gain was not changed during the acquisitions and it was selected to avoid image leakage outside the vessel lumen. The video signal output of the HDI US system was digitized (image acquisition card PCI-1411, National Instruments, Austin, TX, USA) and flow-triggered in real time by a homemade LabView (National Instruments) software. Flow-gated PDI acquisitions were performed at 20 linearly specific instants during the flow period. For each time-gated instant, 50 PDI images were acquired at the rate of one acquisition per cycle, and the average was computed. Averaging was required to have a good definition of the cross-sectional PDI images because no persistence was selected on the US instrument to obtain the best time resolution. The deformation (ellipsoid form of the lumen) of the averaged PDI images as a result of the angle was corrected. Two different sets of acquisitions were performed

with a maximal flow rate of 300 mL/min. First, the minimal flow rate was 0 mL/min (purely forward flow) and the wall filter was set at 50 Hz. Then, the minimal flow was fixed at –100 mL/min (forward and backward flows) with a wall filter of 100 Hz.

### Analytical flow simulations

To analyze how the wall filter could generate signal losses, analytical simulations of pulsatile sinusoidal flow through a straight cylindrical vessel were also performed. The flow was considered laminar and axisymmetric, the fluid incompressible and Newtonian, with properties similar to those used during the *in-vitro* experiments (viscosity of 3.3 cP and density of 1080 kg/m$^3$). The flow rates used for the analytical simulations were those recorded from the electromagnetic flowmeter during the aforementioned *in-vitro* experiments. In the *in-vitro* experiments, the peak Reynolds number did not exceed 600, whereas the Womersley number was 5.7. According to Peacock et al. (1998), the flow was therefore laminar. As a result of the flow and fluid properties, the Navier-Stokes equations were thus reduced to the Womersley equation, which yields the radial and time-dependent longitudinal component of the velocity as a function of the flow rate (Womersley 1955a, 1955b):

$$V_z(r,\ t) = \mathrm{Re}\left\{ \sum_{n=-N}^{N} \frac{Q_n}{\pi R^2} \frac{J_0\left(i^{3/2}\alpha_n\right) - J_0\left(\frac{r}{R}i^{3/2}\alpha_n\right)}{J_0\left(i^{3/2}\alpha_n\right) - \frac{2}{i^{3/2}\alpha_n}J_1\left(i^{3/2}\alpha_n\right)} e^{in\omega t} \right\}$$

$$\text{with} \ \ \alpha_n = R\sqrt{\frac{n\omega\rho}{\mu}}, \quad (1)$$

where $Q_n$ is the $n^{\text{th}}$ harmonic of the flow rate waveform $Q$, $N$ is the number of harmonics, $R$ is the cylinder inner radius (3.98 mm), $i$ is the imaginary unit, $r$ is the radial coordinate, $t$ is time, $\omega$ is $2\pi/T$ where $T$ is the period of the flow, $J_0$ and $J_1$ are the Bessel functions of order zero and one, and $\rho$ and $\mu$ are the density and the dynamic viscosity of the fluid. Re in eqn (1) represents the real part of the function. The number of harmonics $N$ was chosen in such a way that the normalized total error between the actual and reconstructed flow rates was smaller than $10^{-3}$. As described later, theoretical binary PDI images were then constructed from these analytical velocity profiles and compared with the PDI images obtained in the first series of experiments.

### Finite element modeling simulations

Finite element modeling (FEM) simulations of the flow in the vicinity of a cosine-shaped stenosis with an 80% area reduction were also performed with Fluent v. 6.1 (Fluent Inc., Lebanon, NH, USA) to mimic a phys-

iological pathologic condition. The diameter of the feeding vessel was 7.96 mm and the stenosis had a length of 20 mm. The geometry (but not the FEM meshing) was axi-symmetric and the flow was considered turbulent. The mesh of the flow region was composed of 102,102 nodes and 98,830 hexahedral cells, and it was refined near the wall. The segregated solver was used and the value of residual was set at $10^{-3}$ as the criterion of convergence. The time step value was $T/100$ ($T$ = period of one cycle) and six cycles were simulated to eliminate transient flow effects. The $k - \epsilon$ method was used as the turbulent model (Rodi 1993). The fluid dynamic viscosity and density were set at 3.3 cP and 1080 kg/m$^3$, respectively. A null velocity was imposed at the wall (no-slip condition) and a time-dependent velocity profile was imposed as boundary condition at the inlet. Inlet velocities $V_z(r,\ t,\ z = 0)$ were calculated from a typical physiological flow rate (mean flow = 500 mL/min, 70 beats/min, see Fig. 6) using eqn (1). These conditions reflect a normal flow within a human femoral artery.

### Theoretical binary PDI

Based on the velocity fields obtained from the analytical or FEM simulations, the Doppler-shifted frequencies were calculated at each point of the mesh by using the following equation:

$$F(r,\ \varphi,\ z,\ t) = \frac{2F_0}{c}\big[(V_r \sin\varphi + V_\varphi \cos\varphi)\sin\theta_D \\ + V_z \cos\theta_D\big], \quad (2)$$

where $F$ is the Doppler frequency shift, $F_0$ is the US transmitted frequency (4 MHz); $c$ is the sound velocity in human tissues (1540 m/s); $t$ is time; $V_r$, $V_\varphi$ and $V_z$ are the respective cylindrical components of the velocity; and $\theta_D$ is the Doppler angle (70°). The component in square brackets represents the projected velocity on the insonation US axis. Variables $r$, $\varphi$ and $z$ are the cylindrical (radial, angular and longitudinal) coordinates. Only frequencies whose value was greater than the chosen wall filter cutoff frequency contributed to the white pixels of the theoretical binary PDI images. Because $V_r$ and $V_\varphi$ are zero for a laminar flow in an axi-symmetric straight vessel, note that for the analytical simulations, eqn (2) is simply reduced to:

$$F(r,\ \varphi,\ z,\ t) = \frac{2F_0}{c}V_z \cos\theta_D. \quad (3)$$

### Data analyses

Flow-gated PDI averaged acquisitions, obtained with the straight vessel, were compared with the analytical binary PDI images. The images obtained *in vitro* were converted to binary by thresholding. The threshold

value was computed using Otsu's method (Otsu 1979) with MATLAB (The Mathworks Inc., Natick, MA, USA). Otsu's method chooses the threshold so that the intraclass variance of the black and white pixels is minimized (Otsu 1979). The detected lumen area was estimated from the total number of white pixels multiplied by the pixel unit area ( = 0.011 mm$^2$ in this study). Measured lumen areas were compared with those predicted analytically using a linear regression. Regarding the FEM simulations, the PDI signal loss was quantified as the normalized amount of the total volume lost as a result of the wall filter, throughout the cardiac cycle, in the region-of-interest around the stenosis. Four wall filter cutoff frequencies were tested: 25, 100, 500 and 800 Hz.

## RESULTS

*Simulated* vs. *experimental PDI in the straight vessel*

Power Doppler imaging simulations revealed important signal losses within the lumen area at different instants of the flow cycle. Figures 1 and 2 illustrate the results of the two analytical simulations performed with wall filter cutoff frequencies of 50 Hz and 100 Hz, respectively. The cross section of the PDI-detected lumen is represented as a function of time. The black area corresponds to a lack of Doppler signal as a result of the wall filter. Signal losses were central, annular or even covered the entire vessel cross-section. Similar patterns were observed *in vitro*. The annular flow patterns (see Fig. 4 at 40 ms) were induced by the presence of particular velocity profiles looking like the double humps on a camel's back. Such profiles can arise during the deceleration phase when a reverse pressure gradient tends to
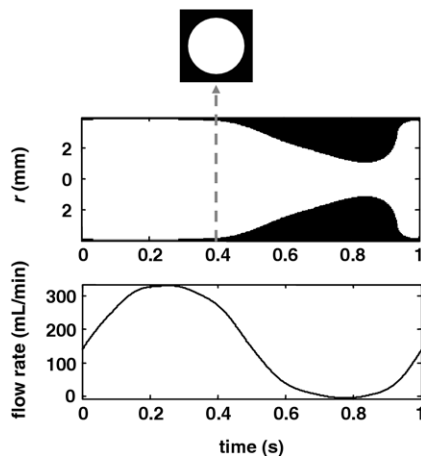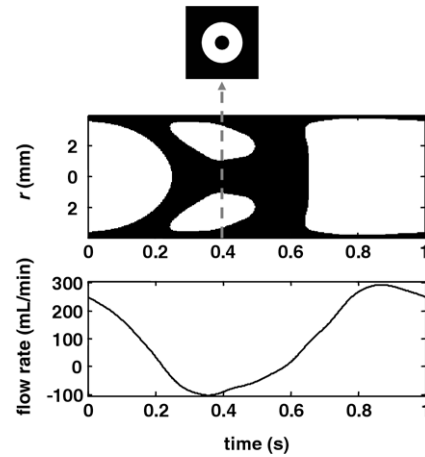


Fig. 2. Top: Simulated binary PDI images as a function of time in the straight vessel (wall filter cut-off frequency = 100 Hz). The snapshot illustrates the complete reconstruction of the theoretical PDI image at time *t* = 0.4 s. Bottom: Corresponding flow rate in mL/min as a function of time.

inverse the flow so that relatively low axial velocities appear. In some circumstances, the wall filter only preserves the two humps (higher velocities), which produce an annular pattern when the flow is axisymmetric. Figures 3 and 4 compare five averaged PDI images obtained *in vitro*, with their corresponding binary and theoretical images, at linearly spaced instants, for the two different



Fig. 1. Top: Simulated binary PDI images as a function of time in the straight vessel (wall filter cut-off frequency = 50 Hz). The snapshot illustrates the complete reconstruction of the theoretical PDI image at time *t* = 0.4 s. Bottom: Corresponding flow rate in mL/min as a function of time.
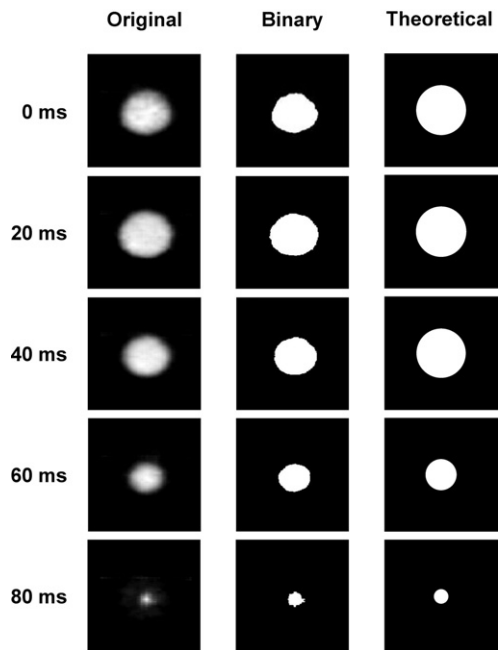


Fig. 3. Five examples among the 20 PDI images available within the flow cycle and their corresponding binary and theoretical images, obtained with the flow rate illustrated in Fig. 1 and a wall filter cut-off frequency of 50 Hz.
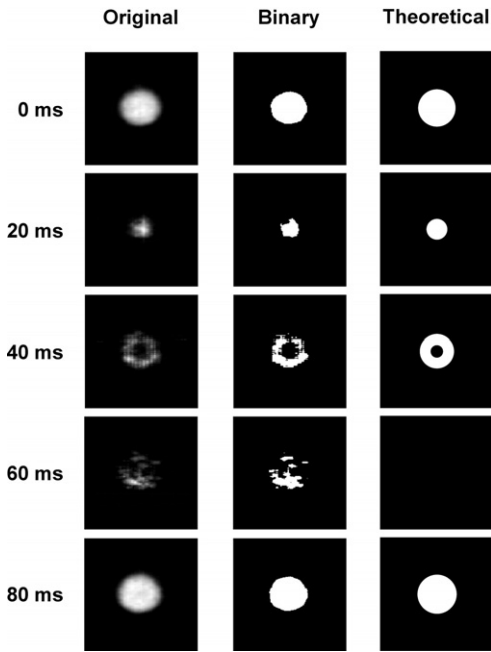
Fig. 4. Five examples among the 20 PDI images available within the flow cycle and their corresponding binary and theoretical images, obtained with the flow rate illustrated in Fig. 2 and a wall filter cut-off frequency of 100 Hz.



Fig. 6. Theoretical PDI images around a severe stenosis under pulsatile flow whose mean value is 500 mL/min. The wall filter cut-off frequency was set at 500 Hz. The white area represents the visible flow.

flow rates depicted in Figs. 1 and 2. There was a very good concordance between measured and predicted PDI binary images. Figure 5 shows the relationship between predicted and measured areas for the whole set of PDI images. The boundary layer as a result of wall friction may be responsible for the underestimation ($y = 0.77 x + 0.73$) of the lumen area. Another factor could be the threshold method used in this study. A good correlation, however, was observed ($r^2 = 0.91$, SEE = 4.60 mm$^2$, $n = 32$), which validates our hypothesis that the wall filter is mostly responsible for the signal losses on signal-gated PDI.
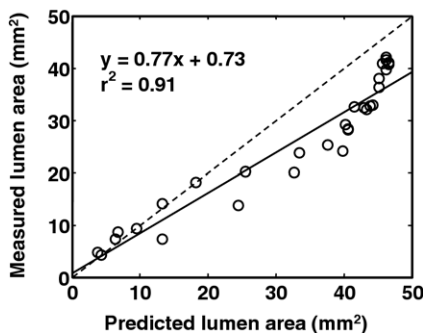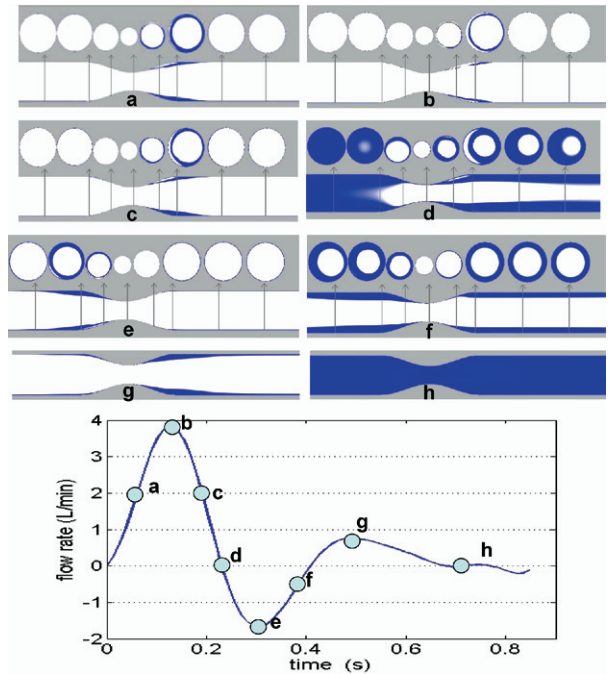


Fig. 5. Relationship between lumen areas (in mm$^2$) measured from the binary *in-vitro* PDI images and those predicted by the analytical simulations.

*Simulated PDI images in an 80% area reduction stenosis*

Figure 6 illustrates simulated PDI images issued from the FEM simulations with a wall filter cut-off frequency of 500 Hz. Figure 7 depicts the measured lumen volume as a function of time for cut-off frequencies ranging from 25 to 800 Hz. As with the straight vessel, important signal losses appeared during the flow cycle, even when the wall filter cut-off frequency was as low as 25 Hz. According to our simulations, the stenosis would be clearly visible at peak flow (time = 0.12 s) whatever the chosen cut-off value of the wall filter. It would become, however, undetectable during diastole with high cut-off values (medium to high wall filters). It should be noted that the loss of visible volume was always higher than 5% with a wall filter cut-off frequency of 800 Hz, even at peak flow. These results show that cardiac-gated PDI imaging may induce severe PDI signal losses that could negatively influence the severity assessment of vascular stenosis. It should be noted that our FEM simulations depicted an ideal hypothetical case (severe stenosis, high flow rate and low wall filter cutoff frequency) so that one can expect to observe more significant signal losses in a typical clinical situation (low to medium flow rates with medium to high wall filters).
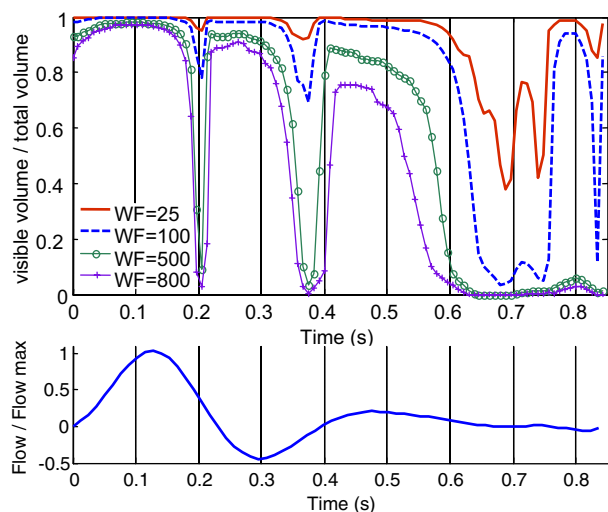
Fig. 7. Top: Normalized visible total volume as a function of time for different wall filter cut-off frequencies (25, 100, 500 and 800 Hz) according to the FEM simulations. Bottom: Corresponding normalized flow rate. Note that extrema appeared for 25 Hz at about $t = 0.7$ s because the flow rate oscillated around 0 L/min (see Fig. 6). At this instant, the flow deceleration was thus successively followed by an acceleration and another deceleration.

## DISCUSSION

### Effects of the wall filter on PDI

Although conventional color Doppler ultrasonography encodes the mean Doppler frequency shift, power Doppler displays the power of the backscattered signal and is, as a consequence, less affected by flow velocity. However, because the low velocity tissue structures may produce high intensity Doppler signals, PDI necessitates the utilization of a high-pass wall filter to remove the resulting artifacts. A few investigators have demonstrated that the wall filter may greatly influence the qualitative information provided by power Doppler images (Jain et al. 1991; Mizushige et al. 1999; Cloutier et al. 2000; Claudon et al. 2001). More precisely, an increase of the filter cut-off frequency has been shown to diminish the signal intensity of power Doppler images (Mizushige et al. 1999), to decrease the detected flow areas (Jain et al. 1991; Claudon et al. 2001) and to underestimate the severity of a vascular stenosis but overestimate its length (Cloutier et al. 2000; Claudon et al. 2001). In the present study, we analyzed the effect of the wall filter on real-time 3-D PDI with a straight vessel and a vessel with a severe stenosis. Consistent with previous studies, we observed that the wall filter can induce an important underestimation of the measured flow area. But more interestingly, our experiments revealed that the wall filter can also produce astonishing annular

patterns, as illustrated in Figs. 2 and 4, or even completely mask any flow signal. Such intriguing results were not observed previously with continuous-averaged PDI imaging because a high time persistence is usually used with this modality. As shown in this study, the effect of wall filter appears to depend on the blood flow velocities, the flow patterns and the degree of filtering so that it would be difficult to quantify each effect precisely. Physicians should be aware of these factors when assessing vessel stenoses.

### Effects of other settings on PDI

It is usually recognized that PDI is relatively angle independent (Rubin 1999), although it was found that the power backscattered by blood can depend on the Doppler angle if the phenomenon of red blood cell aggregation is considered (Fontaine and Cloutier 2003). Interestingly, it has been demonstrated recently *in vitro* that an increase in the pulse repetition frequency (PRF) and in the insonation angle could lead to severe underestimation of stenosis severity (Claudon et al. 2001). To explain these findings, it can be noticed that increasing the insonification angle diminishes the Doppler frequency shift and thereby augments the amount of Doppler signal that falls into the reject band of the wall filter (Rubin 1999), thus inducing PDI signal loss. With regard to the effect of the PRF, it is very important to note that increasing PRF induces an automatic increase of the wall filter cut-off frequency in most US instruments, including the one used by Claudon et al. (2001) (ATL, HDI 3000, Philips Medical System) as well as the one we used in the present study (ATL, HDI 9). The cut-off frequencies indeed vary with the velocity scale; the lowest filter cut-off frequencies cannot be used with the highest velocity ranges and *vice versa* (Kruskal et al. 2004). Here again, the effect of the wall filter has to be considered carefully as the main cause of PDI signal losses.

### Clinical suggestions

Recent engineering advances in US largely improved the temporal and spatial resolutions of US instruments and one may therefore expect that real-time 3-D ultrasonography will become a widespread practice in the near future, especially for the evaluation of cardiac diseases (Claudon et al. 2002). Particularly, dynamic 3-D Doppler imaging has been introduced recently and its performance has been studied during the last five years by a few investigators (Haugen et al. 2000; Claudon et al. 2002; Mehwald et al. 2002; Mori et al. 2002; Herberg et al. 2003; Jones et al. 2003; Sugeng et al. 2003; Brekke et al. 2004; Chaoui et al. 2004). Also, Jones et al. (2003) recently developed some acquisition and visualization algorithms for exploring real-time 3-D power Doppler data. But, in the light of our results, the use of real-time

3-D power Doppler for the assessment of cardiac vessels (aorta, pulmonary artery) or valvular pathologies may be dubious. Our study indeed clearly shows that, even with a low wall filter, very important signal losses can occur during the flow cycle, which makes pointless any analysis of instantaneous power Doppler images to grade stenoses. Rather, we suggest using flow information throughout the complete cardiac cycle by setting persistence at its maximal level because high persistence reduces temporal resolution to obtain a higher spatial resolution. Maximal persistence displays the maximum power and assembles Doppler images sequentially over a given period of acquisition, so as to produce a composite image. The effect of the flow pulsatility can thereby be abolished or reduced and delineation of the flow geometry becomes largely improved. Accordingly, we have previously shown *in vitro* that the selection of a maximum persistence provides the best signal-to-noise ratio of PDI images and considerably reduces the signal loss as a result of the wall filter (Cloutier et al. 2000). It should also be noticed that the delineation of the vessel lumen is highly dependent on spatial resolution, which is at any given frame (or volume) rate, significantly reduced with the 3-D modality compared with 2-D imaging. Besides the effect of the wall filter, a limited spatial resolution may also affect the assessment of arterial stenoses. This drawback, however, is very likely temporary as the resolution of US instruments is incessantly improving. New clinical techniques are also developed to better visualize the blood flow dynamics. For instance, B-mode flow imaging provides images with a better spatio-temporal resolution and gives a better definition of the vessel wall (blood tissue interface) than conventional color flow Doppler imaging (Umemura and Yamada 2001). The B-mode flow imaging modality, however, also includes a wall filter (Chodakauskas et al. 2006) and its benefits over PDI have not yet been investigated.

*Miscellaneous*

According to Fig. 6 and by considering the direct relationship between the wall filter setting and the backscattered power of moving particles contributing to PDI images, one may postulate a new application of this imaging modality for hemodynamic studies. For instance, by properly adjusting the wall filter to reject echoes from blood moving in a given range of low velocities, one may use real-time 3-D PDI to estimate the position of the shear layer (recirculation zone) downstream of a stenosis. As seen in Fig. 6, the loss of signal downstream of the obstruction varies according to the timing within the flow cycle. Consequently, this may be a way to track and quantify the magnitude of oscillatory flow, which is known to play a role in the development of atherosclerosis (Cheng et al. 2006).

## CONCLUSIONS

In the present study, we demonstrated that signal losses on PDI images were attributed to the wall filter. In a straight tube, a correlation $r^2$ of 91% was obtained between flow-gated experimental measures of lumen areas and theoretical predictions, thus confirming the impact of the wall filter on PDI signal losses and reductions of measured lumen areas. Finite element simulations were also presented to show the effect of the wall filter on artifactual reductions of instantaneous estimates of lumen areas around a severe stenosis. The PDI signal losses were central, annular and even covered the entire vessel cross section. Our results thus make the use of real-time 3-D power Doppler questionable for the assessment of cardiovascular pathologies. Clinicians should therefore be aware of this cause of signal loss to properly interpret power Doppler angiographic images.

## REFERENCES

Allard L, Cloutier G, Durand LG. Effect of the insonification angle on the Doppler backscattered power under red blood cell aggregation conditions. IEEE Trans Ultrason Ferroelect Freq Control 1996;43:211–219.

Allard L, Cloutier G. Power Doppler ultrasound scan imaging of the level of red blood cell aggregation: An in vitro study. J Vasc Surg 1999;30:157–168.

Bluth EI, Sunshine JH, Lyons JB, Beam CA, Troxclair LA, Althans-Kopecky L, Crewson PE, Sullivan MA, Smetherman DH, Heidenreich PA, Neiman HL, Burkhardt JH. Power Doppler imaging: Initial evaluation as a screening examination for carotid artery stenosis. Radiology 2000;215:791–800.

Bluth EI. Power Doppler imaging to evaluate flow-limiting stenoses. Radiology 2001;221:557–558.

Brekke S, Tegnander E, Torp HG, Eik-Nes SH. Tissue Doppler gated (TDOG) dynamic three-dimensional ultrasound imaging of the fetal heart. Ultrasound Obstet Gynecol 2004;24:192–198.

Chaoui R, Hoffmann J, Heling KS. Three-dimensional (3D) and 4D color Doppler fetal echocardiography using spatio-temporal image correlation (STIC). Ultrasound Obstet Gynecol 2004;23:535–545.

Cheng C, Tempel D, van Haperen R, van der Baan A, Grosveld F, Daemen MJAP, Krams R, de Crom R. Atherosclerotic lesion size and vulnerability are determined by patterns of fluid shear stress. Circulation 2006;113:2744–2753.

Chodakauskas T, Kleveland T, Bjaerum S. Blood flow imaging. GE Healthcare documentation 2006:1–4.

Claudon M, Winninger D, Briancon S, Pesque P. Power Doppler US: Evaluation of the morphology of stenoses with a flow phantom. Radiology 2001;218:109–117.

Claudon M, Tranquart F, Evans DH, Lefevre F, Correas M. Advances in ultrasound. Eur Radiol 2002;12:7–18.

Cloutier G, Qin Z, Garcia D, Soulez G, Oliva V, Durand LG. Assessment of arterial stenosis in a flow model with power Doppler angiography: Accuracy and observations on blood echogenicity. Ultrasound Med Biol 2000;26:1489–1501.

Fontaine I, Cloutier G. Modeling the frequency dependence (5–120 MHz) of ultrasound backscattering by red cell aggregates in shear flow at a normal hematocrit. J Acoust Soc Am 2003;113:2893–2900.

Griewing B, Morgenstern C, Driesner F, Kallwellis G, Walker ML, Kessler C. Cerebrovascular disease assessed by color-flow and power Doppler ultrasonography. Comparison with digital subtraction angiography in internal carotid artery stenosis. Stroke 1996;27:95–100.

Guo Z, Fenster A. Three-dimensional power Doppler imaging: A phantom study to quantify vessel stenosis. Ultrasound Med Biol 1996;22:1059–1069.

Guo Z, Durand LG, Allard L, Cloutier G, Fenster A. In vitro evaluation of multiple arterial stenoses using three-dimensional power Doppler angiography. J Vasc Surg 1998;27:681–688.

Haugen BO, Berg S, Brecke KM, Samstad SO, Slordahl SA, Skjaerpe T, Torp H. Velocity profiles in mitral blood flow based on three-dimensional freehand colour flow imaging acquired at high frame rate. Eur J Echocardiogr 2000;1:252–256.

Helenon O, Correas JM, Chabriais J, Boyer JC, Melki P, Moreau JF. Renal vascular Doppler imaging: Clinical benefits of power mode. Radiographics 1998;18:1441–1454.

Herberg U, Goldberg H, Breuer J. Dynamic free-hand three-dimensional fetal echocardiography gated by cardiotocography. Ultrasound Obstet. Gynecol 2003;22:493–502.

Jain SP, Fan PH, Philpot EF, Nanda NC, Aggarwal KK, Moos S, Yoganathan AP. Influence of various instrument settings on the flow information derived from the power mode. Ultrasound Med Biol 1991;17:49–54.

Jones MG, Shipley JA, Robinson TM. Visualisation of 4-D colour and power Doppler data. Ultrasound Med Biol 2003;29:1735–1747.

Koga M, Kimura K, Minematsu K, Yamaguchi T. Diagnosis of internal carotid artery stenosis greater than 70% with power Doppler duplex sonography. AJNR Am J Neuroradiol 2001;22:413–417.

Kruskal JB, Newman PA, Sammons LG, Kane RA. Optimizing Doppler and color flow US: Application to hepatic sonography. Radiographics 2004;24:657–675.

Kuwa T, Cancio LC, Sondeen JL, Matylevich N, Jordan BS, McManus AT, Goodwin CW. Evaluation of renal cortical perfusion by non-invasive power Doppler ultrasound during vascular occlusion and reperfusion. J Trauma 2004;56:618–624.

Manganaro A, Ando G, Salvo A, Consolo A, Coppolino F, Giannino D. A comparison of power Doppler with conventional sonographic imaging for the evaluation of renal artery stenosis. Cardiovasc. Ultrasound 2004;2:1; www.Cardiovascularultrasound.com.

Masugata H, Cotter B, Peters B, Ohmori K, Mizushige K, DeMaria AN. Assessment of coronary stenosis severity and transmural perfusion gradient by myocardial contrast echocardiography: Comparison of gray-scale B-mode with power Doppler imaging. Circulation 2000;102:1427–1433.

Masugata H, DeMaria AN, Peters B, Lafitte S, Strachan GM, Kwan OL, Ohmori K, Mizushige K, Kohno M. Difference of optimal dose of contrast agent between gray-scale and power Doppler imaging in assessing graded coronary stenosis by myocardial contrast echocardiography. Invest Radiol 2003;38:550–558.

Mehwald PS, Rusk RA, Mori Y, Li XN, Zetts AD, Jones M, Sahn DJ. A validation study of aortic stroke volume using dynamic 4-dimensional color Doppler: An in vivo study. J Am Soc Echocardiogr 2002;15:1045–1050.

Mizushige K, Ueda T, Yuba M, Seki M, Ohmori K, Nozaki S, Matsuo H. Dependence of power Doppler image on a high pass filter instrumented in ultrasound machine. Ultrasound Med Biol 1999;25:1389–1393.

Mori Y, Rusk RA, Jones M, Li XN, Irvine T, Zetts AD, Sahn DJ. A new dynamic three-dimensional digital color Doppler method for quantification of pulmonary regurgitation: Validation study in an animal model. JACC 2002;40:1179–1185.

Muller M, Ciccotti P, Reiche W, Hagen T. Comparison of color-flow Doppler scanning, power Doppler scanning, and frequency shift for assessment of carotid artery stenosis. J Vasc Surg 2001;34:1090–1095.

Nagao M, Murase K, Saeki H, Mochizuki T, Sugata S, Ikezoe J. Pulsating renal blood flow distribution measured using power Doppler ultrasound: Correlation with hypertension. Hypertens Res 2002;25:697–702.

Otsu N. A threshold selection method from gray-level histograms. IEEE Trans Syst Man Cyber 1979;9:62–66.

Peacock J, Jones T, Tock C, Lutz R. The onset of turbulence in physiological pulsatile flow in a straight tube. Exp Fluids 1998;24:1–9.

Poepping TL, Nikolov HN, Rankin RN, Lee M, Holdsworth DW. An in vitro system for Doppler ultrasound flow studies in the stenosed carotid artery bifurcation. Ultrasound Med Biol 2002;28:495–506.

Rocchi G, Fallani F, Bracchetti G, Rapezzi C, Ferlito M, Levorato M, Reggiani LB, Branzi A. Non-invasive detection of coronary artery stenosis: A comparison among power-Doppler contrast echo, 99Tc-Sestamibi SPECT and echo wall-motion analysis. Coronary Artery Dis 2003;14:239–245.

Rodi W. Turbulence models and their application in hydraulics. A state of the art review. Brookfield, Rotterdam, 1993.

Rubin JM, Adler RS. Power Doppler expands standard color capability. Diagn Imaging (San Fran) 1993;15:66–69.

Rubin JM, Bude RO, Carson PL, Bree RL, Adler RS. Power Doppler US: A potentially useful alternative to mean frequency-based color Doppler US. Radiology 1994;190:853–856.

Rubin JM. Power Doppler. Eur Radiol 1999;9(Suppl 3):S318–S322.

Schmidt P, Sliwka U, Simon SG, Noth J. High-grade stenosis of the internal carotid artery assessed by color and power Doppler imaging. J Clin Ultrasound 1998;26:85–89.

Steinke W, Meairs S, Ries S, Hennerici M. Sonographic assessment of carotid artery stenosis. Comparison of power Doppler imaging and color Doppler flow imaging. Stroke 1996;27:91–94.

Steinke W, Ries S, Artemis N, Schwartz A, Hennerici M. Power Doppler imaging of carotid artery stenosis. Comparison with color Doppler flow imaging and angiography. Stroke 1997;28:1981–1987.

Sugeng L, Spencer KT, Mor-Avi V, DeCara JM, Bednarz JE, Weinert L, Korcarz CE, Lammertin G, Balasia B, Jayakar D, Jeevanandam V, Lang RM. Dynamic three-dimensional color flow Doppler: An improved technique for the assessment of mitral regurgitation. Echocardiography 2003;20:265–273.

Umemura A, Yamada K. B-mode flow imaging of the carotid artery. Stroke 2001;32:2055–2057.

Villanueva FS, Gertz EW, Csikari M, Pulido G, Fisher D, Sklenar J. Detection of coronary artery stenosis with power Doppler imaging. Circulation 2001;103:2624–2630.

Winsberg F. Power Doppler US [letter]. Radiology 1995;195:873.

Womersley JR. Mathematical theory of oscillating flow in an elastic tube. J Physiol 1955a;127:37–44.

Womersley JR. Method for the calculation of velocity, rate of flow and viscous drag in arteries when the pressure gradient is known. J Physiol 1955b;127:553–563.

Yoon DY, Choi BI, Kim TK, Han JK, Yeon KM. Influence of instrument settings on flow signal and background noise in power Doppler US. An experimental study using a flow phantom with hyperechoic background. Invest Radiol 1999;34:781–784.

Yu ACH. Eigen-based signal processing methods for ultrasound color flow imaging. PhD thesis, Department of Electrical and Computer Engineering, University of Toronto, 2007.

Yurdakul M, Tola M, Cumhur T. B-flow imaging of internal carotid artery stenosis: Comparison with power Doppler imaging and digital subtraction angiography. J Clin Ultrasound 2004;32:243–248.